Wind and Structures, *Vol. 25, No. 2 (2017) 101-129*
DOI: https://doi.org/10.12989/was.2017.25.2.101

Multi-dimensional extreme aerodynamic load calculation in super-large cooling towers under typical four-tower arrangements

Shitang Ke[*1,2], Hao Wang[1,2a] and Yaojun Ge[3b]

[1]*Department of Civil Engineering, Nanjing University of Aeronautics and Astronautics, Yudao Road 29, Nanjing 210016, China*
[2]*Jiangsu Key Laboratory of Hi-Tech Research for Wind Turbine Design, Nanjing University of Aeronautics and Astronautics, Nanjing 210016, China*
[3]*State Key Laboratory for Disaster Reduction in Civil Engineering, Tongji University, Siping Road 1239, Shanghai 200092, China*

(Received April 17, 2017, Revised July 17, 2017, Accepted July 19, 2017)

Abstract. Local transient extreme wind loads caused by group tower-related interference are among the major reasons that lead to wind-induced damage of super-large cooling towers. Four-tower arrangements are the most commonly seen patterns for super-large cooling towers. We considered five typical four-tower arrangements in engineering practice, namely, single row, rectangular, rhombic, L-shaped, and oblique L-shaped. Wind tunnel tests for rigid body were performed to determine the influence of different arrangements on static and dynamic wind loads and extreme interference effect. The most unfavorable working conditions (i.e., the largest overall wind loads) were determined based on the overall aerodynamic coefficient under different four-tower arrangements. Then we calculated the one-, two- and three-dimensional aerodynamic loads under different four-tower arrangements. Statistical analyses were performed on the wind pressure signals in the amplitude and time domains under the most unfavorable working conditions. On this basis, the non-Gaussian distribution characteristics of aerodynamic loads on the surface of the cooling towers under different four-tower arrangements were analyzed. We applied the Sadek-Simiu procedure to the calculation of two- and three-dimensional aerodynamic loads in the cooling towers under the four-tower arrangements, and the extreme wind load distribution patterns under the most unfavorable working conditions in each arrangement were compared. Finally, we proposed a uniform equation for fitting the extreme wind loads under the four-tower arrangements; the accuracy and reliability of the equation were verified. Our research findings will contribute to the optimization of the four-tower arrangements and the determination of extreme wind loads of super-large cooling towers.

Keywords: four-tower arrangement; super-large cooling tower; wind tunnel test; non-Gaussian distribution; multi-dimensional extreme wind load; interference effect

*Corresponding author, Associate Professor, E-mail: keshitang@nuaa.edu.cn
[a] Ph.D. Student, Email: wanghaonuaa@nuaa.edu.cn
[b] Professor, Email: yaojunge@tongji.edu.cn

Copyright © 2017 Techno-Press, Ltd.
http://www.techno-press.org/?journal=was&subpage=8 ISSN: 1226-6116 (Print), 1598-6225 (Online)

1. Introduction

Group tower-induced interference is a classical issue in the field of wind engineering. Investigations into this topic will offer both theoretical and practical values. In 1965 the 8 cooling towers arranged in a two-row rhombic pattern at the Ferrybridge power station in England collapsed during strong wind with a five year return period. Many surveys have been conducted into the reasons of the wind-induced damage (Bearman 1967, Swartz *et al*. 1985, Pope 1994), and the following reasons are proposed: (1) The design wind speed specified in the codes of England was not used; (2) The amplification of surface wind loads of the cooling towers due to group tower-induced interference was not considered; (3) The tensile reinforcements in the meridional direction, which were designed according to the average wind pressures, could not withstand the actual extreme wind loads; (4) Only one central reinforcing mesh was used in the tower tube, which could not withstand the action of bending moment in the tower tube. Among the above reasons, local transient extreme wind loads caused by group tower-induced interference are still the leading cause of wind-induced damage of large cooling towers. At present, group towers of power plants are usually built in four-tower arrangements. However, the existing cooling tower design codes (DL/T 5339-2006 2006, GB/T 50102-2014, 2014, VGB-Guideline 2005) rarely provide the extreme wind load distributions under the four-tower arrangement. Few studies have been done to understand the mechanism of group tower-induced interference under the typical four-tower arrangements.

Regarding the topic of group tower-induced interfernece, some studies (Niemann and Kopper 1998, Portela and Godoy 2005) performed a series of wind tunnel tests to obtain the distributions of mean wind pressure and pulsating wind pressure on the surface of the cooling towers under different distances between the towers. Others (Sun and Gu 1995, Orlando 2001, Li *et al*. 2013) studied the distributions of interference factor of wind pressure under the two-tower arrangement through wind tunnel tests and CFD technique and plotted the variations of the overall force coefficient with wind angle. In some researches (Moon *et al*. 2008, Rajan *et al*. 2013), two patterns of three-tower arrangements were considered in the wind tunnel tests to obtain the values of wind pressure. Based on the experimental data, the values of interference factor and the wind-induced response characteristics were determined under the three-tower arrangements. Ke *et al*. (2015) performed wind tunnel tests to measure the pressures of rigid body and aeroelastic vibration under the oblique L-shaped four-tower arrangement with the consideration of the topographic factor. Furthermore, the effect of group tower-induced interference on the wind-induced stability of the cooling towers was discussed based on the overall resistance coefficient.

Some systemic studies have been conducted regarding the pulsating wind loads acting on a single cooling tower (Viladkar *et al*. 2006, Wittek and Grote 2015). The results indicated conspicuous non-Gaussian distribution characteristics of local wind pressure probability in large cooling towers. This feature contributed to the local instability and strength failure of the cooling tower. Ke and Ge (2015) applied the Sadek-Simiu procedure to estimate the peak factor of pulsating wind pressure and extreme wind pressure distribution in a single cooling tower. Other scholars (Karaqkas *et al*. 2016, Cheng *et al*. 2015) performed wind tunnel tests and field measurements to understand the distributions and forming mechanism of pulsating wind pressure on the surface of the cooling tower. Their works lay the basis for other simulation of pulsating wind pressure in a single cooling tower.

As seen from above, many systemic studies have been done regarding the interference effect related to the group cooling towers and the estimation of extreme wind pressures in a single tower.

Table 1 Geometrical dimension of the cooling tower

Part	Size(unit: m)	Schematic of the measuring points (unit: m)
Tower height	220	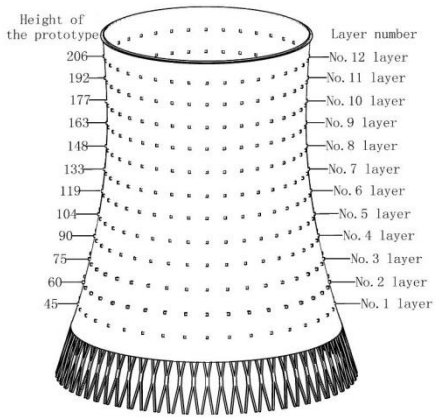
Throat altitude	165	
Inlet altitude	31	
Top diameter	128	
Bottom diameter	185	
Throat diameter	123	
Thickness	0.39-1.85	
Rect. cross sections of columns	1.7×1.0	

But the distributions and forming mechanism of multi-dimensional extreme aerodynamic loads under the typical four-tower arrangement are rarely known. To this end, we took the super-large cooling tower as the research subject, which is the highest cooling tower ever built, standing 220 m. A total of 353 working conditions under a single tower, double towers, and four towers respectively arranged in five patterns (single row, rectangular, rhombic, L-shaped, oblique L-shaped) were discussed through wind tunnel tests on a rigid model. Statistical procedures were performed in the amplitude and time domains to obtain the non-Gaussian distribution characteristics of aerodynamic loads on the surface of the cooling towers under the four-tower arrangement. Moreover, extreme aerodynamic loads under the different four-tower arrangements were calculated using the Sadek-Simiu procedure. Finally, we proposed a method for evaluating multi-dimensional extreme aerodynamic loads under the interference effect of four-tower arrangement. The accuracy and reliability of the method were verified through experiments.

2. Wind tunnel tests and data processing

2.1 An overview of the project

The tower height was 220 m, with throat altitude of 165 m and inlet altitude of 30.75 m; the top diameter was 128 m, the throat diameter 123 m and the bottom diameter 185 m. The tower was supported by 64 pairs of X-shaped pillars which were connected to the annular plate foundation.

The X-shaped pillars were of a rectangular cross section measuring 1.7 m×1.0 m.

The scale ratio of the model used for wind tunnel tests was 1:450. The model was made of acrylic to ensure sufficient stiffness and strength. Along the meridional direction 12 circles of external pressure measuring points were arranged on the tower surface. For each circle 36 measuring points were uniformly and clockwise distributed in the circumferential direction. Thus there were 432 measuring points, as shown in Fig. 1.

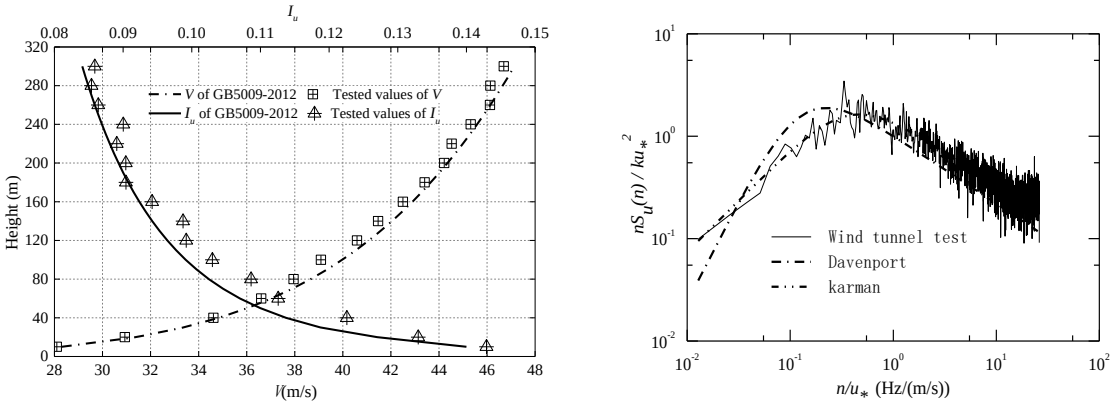

(a) Mean wind speed and turbulence (b) Pulsating wind spectrum

Fig. 1 Simulation results of wind characteristics in BLWT

The pressure taps were connected with the measurement system through PVC tubing. To avoid the distortion of the dynamic pressure, the signals had been modified using the transfer function of the tubing systems. A DSM 3000 scan valve system was used to measure the wind pressures on the rigid model of the tower. The pressure signals were sampled at 312.5 Hz.

2.2 Wind field simulation

The wind tunnel was a closed jet return flow tunnel with a rectangular cross section. The working section was 5 m wide and 4.5 m high. The wind field was simulated as the category B terrain according to the Load Code for the Design of Building Structures (GB50009-2012, 2012).

The main indicators of wind field simulation were mean wind speed profile, turbulence intensity profile and along-wind pulsating wind spectrum. The triangle wedge and roughness element were placed in front of the incoming flow to simulate the wind field. Fig. 1 shows the simulation result. It can be seen that the simulated wind field satisfied the experimental requirements.

2.3 Reynolds number simulation

Ten levels of surface roughness were tested in wind tunnel tests for the correction of Reynolds number effect: 1) Smooth surface; 2)With 16 trip wires having a width of 2 mm uniformly attached to the tower surface; 3) With 32 trip wires having a width of 2 mm uniformly attached to the tower surface; 4) With 64 trip wires having a width of 2 mm uniformly attached to the tower surface; 5) With 1 layer of 36 rough paper tapes having a width of 5 mm uniformly attached to the tower surface; 6) With 2 layers of 36 rough paper tapes having a width of 5 mm uniformly attached to the tower surface; 7) With 2/3 layers of 36 rough paper tapes having a width of 5 mm intermittently attached to the tower surface; 8) With 3 layers of 36 rough paper tapes having a width of 5 mm uniformly attached to the tower surface; 9) With 3/4 layers of 36 rough paper tapes having a width of 5 mm intermittently attached to the tower surface; 10) With 4 layers of 36 rough paper tapes having a width of 5 mm uniformly attached to the tower surface. The main parameters

compared by simulation of Reynolds number effect were minimal shape coefficient, shape coefficient of the wake region, angle corresponding to zero shape coefficient, angle corresponding to minimal shape coefficient and angle at the point of separation (Farell *et al*. 1976, Suna and Zhoub 1983, Ke *et al*. 2013).

Wind pressure obtained from the pitot tube was used to calculate the non-dimensional pressure coefficients. The shape coefficient can be obtained was determined by

$$Cp_{i,\theta} = \frac{P_{i,\theta} - \bar{P}_s}{\bar{P}_{t,h} - \bar{P}_s} / \left(\frac{Z_i}{h}\right)^{2\alpha} = \frac{P_{i,\theta} - \bar{P}_s}{0.5\rho \bar{V}_h^2} / \left(\frac{Z_i}{h}\right)^{2\alpha} \tag{1}$$

where $Cp_{i,\theta}$ is the shape coefficient at the ith measuring point in wind direction θ, $P_{i,\theta}$ is the pressure at the ith measuring point, $\bar{P}_s$ and $\bar{P}_{t,h}$ are the static pressure and total pressure of the pitot tube at reference points in the wind tunnel, respectively. $\bar{V}_h$ is the wind velocity at reference point. Z_i is the height of ith measuring point, α is the exponent of the mean wind speed profile for terrain category B.

Fig. 2 shows the distribution curves of normalized shape coefficient at the throat under different surface roughness, and they were compared against the standard curves (DL/T 5339-2006 2006, GB/T 50102-2014 2014). It can be seen from the figure that the Reynolds number effect was best simulated by uniformly attaching 4 layers of rough paper tapes. Fig. 3 is the picture of the model used for the formal tests.

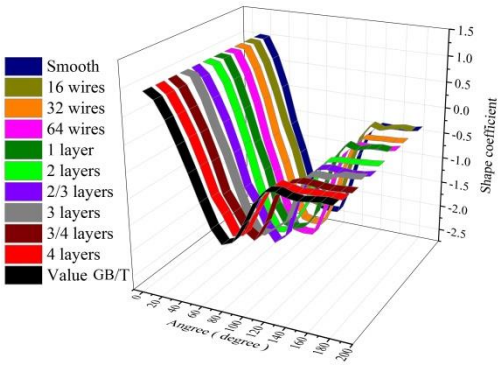

Fig. 2 Comparison of Cp between wind tunnel tests and target curve

Fig. 3 Diagram of simulation of Reynolds effect measure

2.4 Working conditions under the tests

Six arrangements of the cooling towers were tested in the wind tunnel, namely, double towers and four-tower arrangements in different patterns (single row, rectangular, rhombic, L-shaped, oblique L-shaped). For each arrangement, measurement was performed with an increment of 22.5° within the wind direction ranging from 0 to 360°. Sixteen wind directions were selected.

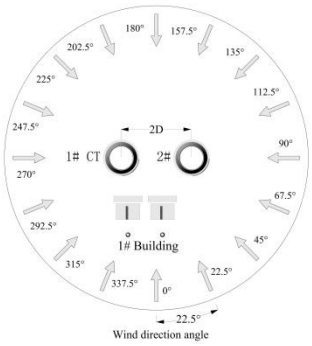

(a) Double tower

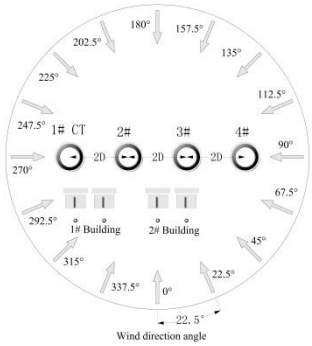

(b) Four towers in a row

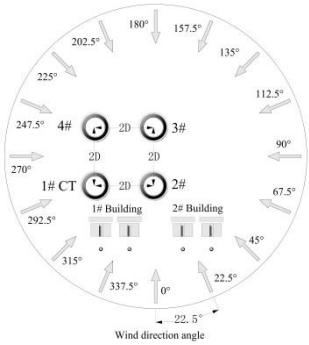

(c) Four towers in a rectangular pattern

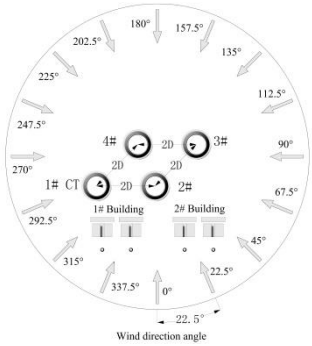

(d) Four towers in a rhombic pattern

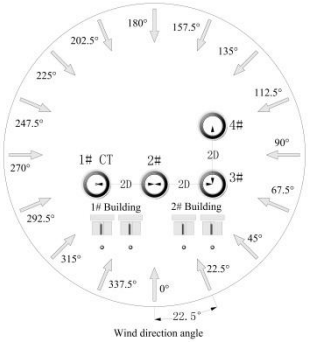

(e) Four towers in an L-shaped pattern

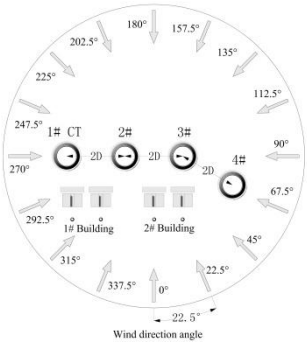

(f) Four towers in an oblique L-shaped pattern

Fig. 4 Diagram of layouts of grouped towers

The center distances for large cooling towers in existing design codes (DL/T 5339-2006 2006, GB/T 50102-2014, 2014, VGB-Guideline 2005) are recommended as 1.5D ~ 2.5D, with D being the bottom diameter. Studies (Niemann and Kopper 1998, Orlando 2001, Zhang *et al*. 2016) have shown that the controlling case of cooling tower group is influenced considerably by arrangement format and relative location but negligibly by center distances. This paper aims to explore the size effect and interference mechanism of the interference effect of different four-tower combination under the fixed tower space. Therefore, the representative tower spacing (2D) was selected in this paper. To realistically simulate the actual layout, several interference structures were arranged near the group towers. Fig. 4 shows the planar views of each arrangement. The maximum blockage rate for the group towers was 3.22%, which satisfied the standard for wind tunnel testing (JSJ/T 338-2014 2014, ASCE 49-12-2012).

2.5 Date treatment

Assurance coefficient should be considered for estimating extreme pulsating wind load in engineering design

$$Cp_{i,\max}=Cp_{i,\mathrm{mean}}+sign(Cp_{i,\mathrm{mean}})\times g\times\sigma_i \tag{2}$$

where $Cp_{i,\max}$ is extreme shape coefficient; $Cp_{i,\mathrm{mean}}$ is mean shape coefficient; $sign(Cp_{i,\mathrm{mean}})$ is the symbolic vector of $Cp_{i,\mathrm{mean}}$; σ_i is root variance of shape coefficient which is corresponding to the *i*th pressure tap; g is assurance coefficient, also known as the peak factor.

3. Analysis on the interference effects

3.1 A quantification method

The interference factor (*IF*) is commonly used to assess the interference effects imposed by the surrounding structures onto the target tower. It is given by

$$IF=\frac{\text{Wind loads of the structure with interference}}{\text{Wind loads of the structure without interference}} \tag{3}$$

There are several types of interference factors, including maximum positive pressure-related interference factor, minimum negative pressure-related interference factor, resistance coefficient-related interference factor, and lift coefficient-related interference factor. Studies (Niemann and Kopper 1998, Orlando 2001, Cheng *et al*. 2013, Ke *et al*. 2015) have shown that the maximum positive pressure-related interference factor and the maximum negative pressure-related interference factor only consider the local distribution of wind pressure on the structure surface; they are not fully applicable as the structural design indicators for cooling towers with a 3D shell structure. For the sake of structural safety and economic rationality, we chose the interference factors based on resultant force coefficient for the study of interference effect in this paper. Therefore, we synthesized the resultant force coefficient from the overall resistance coefficient and lift coefficient (Eq. (4)) so as to calculate the mean interference factor, dynamic interference factor and extreme interference factor.

$$C_T = \sqrt{C_D^2 + C_L^2} \tag{4}$$

where C_T, C_D and C_L are the resultant force coefficient, resistance coefficient and lift coefficient of the cooling towers, respectively.

Figs. 5 and 6 provide the time history of resultant force coefficients and the corresponding probability density curves for a single tower and a typical four-tower arrangement (2# tower in rhombic arrangement with a wind direction of 247.5°). The skewness and kurtosis of the resultant force coefficient for a single tower are 0.34 and 3.07, respectively; for the four-tower arrangement, they are 0.43 and 3.45, respectively. Moreover, the probability distributions of the resultant force coefficient for the single tower and the four-tower arrangement obey the normal distribution. Resultant force coefficient is synthesized from all wind pressures at the measuring points on the surface of the cooling towers. According to the central limit theorem (Brosamler 1988), the probability density distribution of resultant force coefficient is closer to Gaussian distribution than the wind pressure signals of a single measuring point. The value of the peak factor is taken as 3.5 in the calculation of extreme resultant force coefficient (GB50009-2012, 2012, Ke and Ge 2015).

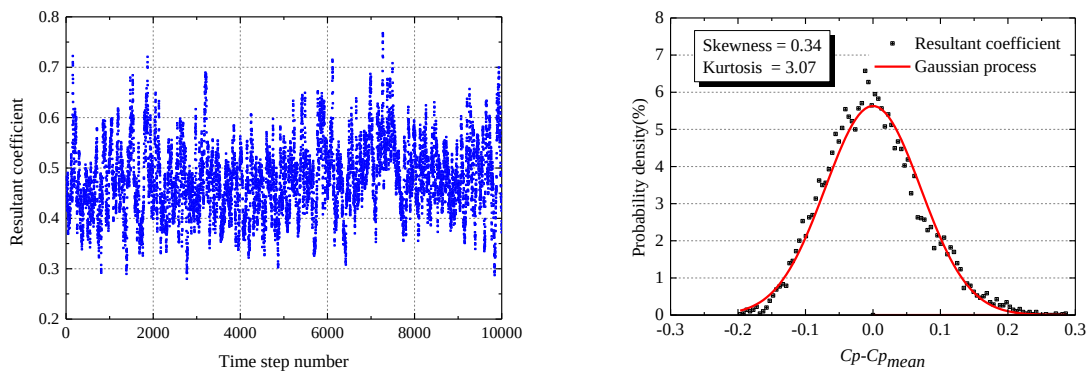

(a) Time history (b) Probability density curve

Fig. 5 Time history curve and probability density curve of resultant force coefficient under a single tower

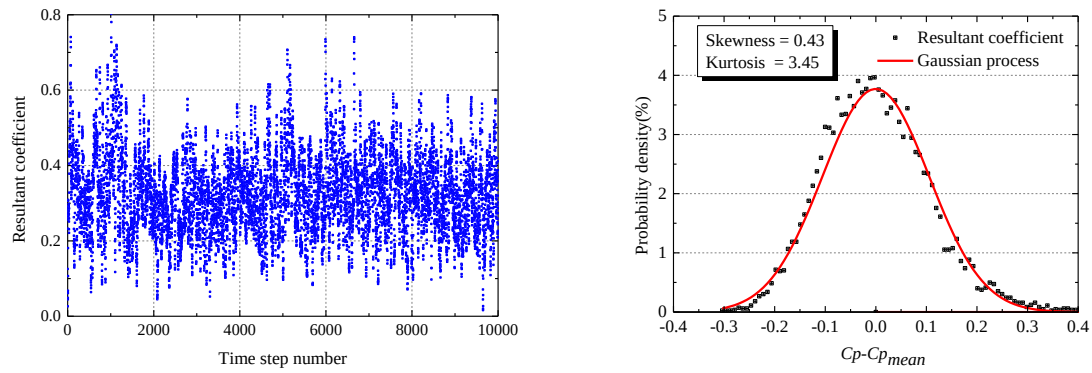

(a) Time history (b) Probability density curve

Fig. 6 Time history curve and probability density curve of resultant force coefficient under four-tower arrangement

3.2 Most unfavorable interference effects

We calculated the mean interference factor (*MIF*), dynamic interference factor (*DIF*) and extreme interference factor (*EIF*) based on the time history of resultant force coefficient. These three interference factors are defined as follows

$$MIF = \frac{G(C_{Tmean})}{S(C_{Tmean})} \tag{5}$$

$$DIF = \frac{G(C_{Trms})}{S(C_{Trms})} \tag{6}$$

$$EIF = \frac{G(C_{T\max})}{S(C_{T\max})} \tag{7}$$

where $G(*)$ and $S(*)$ are the eigenvalues of the resultant force coefficient under the four-tower arrangement and a single tower, respectively.

Fig. 7 shows the maximum values of *MIF*, *DIF* and *EIF* as well as the occurrence positions under different four-tower arrangements. The *y*-axis represents the interference factor, and x-axis different arrangements; the position parameters are the serial number of towers (#) and wind angle (°) under the most unfavorable working conditions. It can be seen that (1) the maximum interference factors under the double tower arrangement are all smaller than those under the four-tower arrangements; the maximum interference factors across different arrangements are generally found in the 2# tower. This indicates the amplification of the wind loads imposed by the towers under construction to those already built up; (2) The values of *DIF* are the highest, and some are above 2.0 under the most unfavorable working conditions; the values of *MIF* are the smallest under all arrangements. Of different four-tower arrangements, the most unfavorable condition occur to 2# tower, which is subjected to considerable interferences imposed by the surrounding towers; so the working conditions of 2# tower were the control working conditions under the four-tower arrangements. Therefore, the following estimation of extreme aerodynamic loads was performed based on 2# tower. Extreme interference factor not only reflects the shielding effect for the target tower in the downstream of the interference towers, but also the amplification of wind loads for the target tower located in the downstream of the slit between the two towers. Here the working condition with maximum *EIF* was considered the most unfavorable across different tower arrangements.

Fig. 8 provides the layout of five typical four-tower arrangements. The positions of 1# and 2# towers were fixed and they were considered as a whole (group tower A), and 3# and 4# towers formed group tower B. The difference of the five four-tower arrangements was the changing of relative position between group towers A and B. The angle of the line connecting the centers of group towers A and B with respect to the X-axis was defined as the characteristic angle α (absolute value); it was α=18° in the L-shaped pattern, as shown in Fig. 8. Fig. 9 is the schematic of the correlation between maximum *EIF* and characteristic angle α under the four-tower arrangements. A good linear correlation is indicated from the figure, the coefficient of correlation being 0.99. The regression relation can be represented by Eq. (8), and it will be valid for the selected reference spacing of 2D and the four tower arrangements considered. It can be observed that as the characteristic angle increases ($\alpha \leq 90°$), the interference effect related to overall wind load will increase persistently under the four-tower arrangements.

$$Max(EIF) = 1.278 + 0.0022\alpha \tag{8}$$

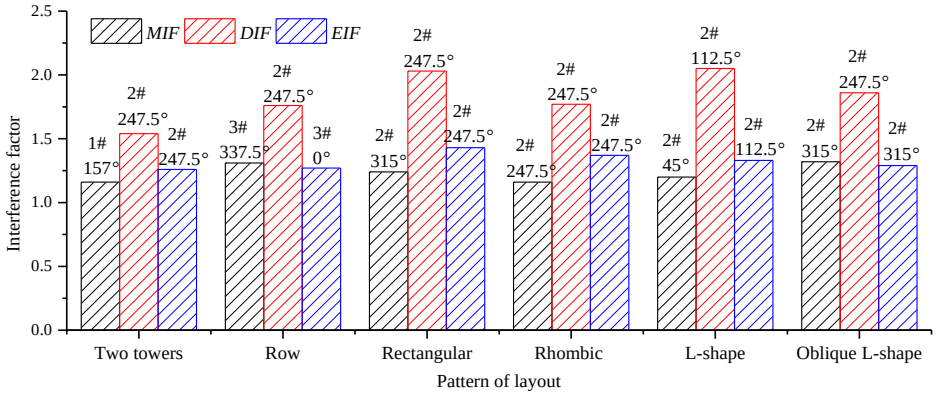

Fig. 7 Maximum interference factors under double-tower arrangement and five four-tower arrangements

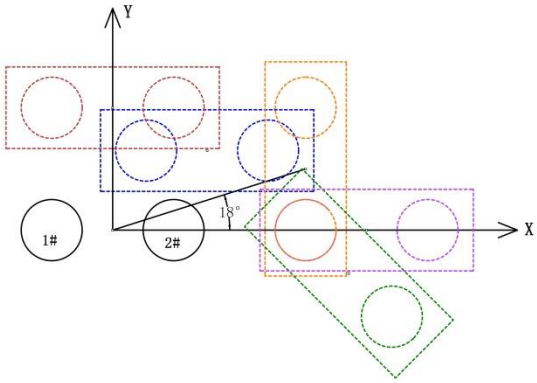

Fig. 8 Schematic of five typical four-tower arrangements

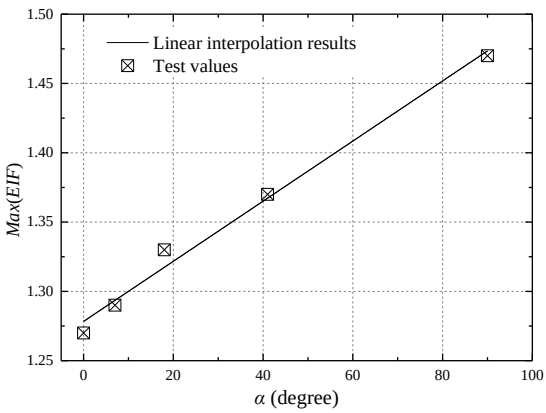

Fig. 9 Schematic diagram of the correlation between the characteristic angle (α) and the maximum EIF of five typical four-tower arrangements

4. Local distribution of aerodynamic loads

4.1 Average wind loads

Fig. 10 shows the distribution curves of 2D shape coefficient under the most unfavorable working conditions under the single-tower and five four-tower arrangements. The results in the figure are the averages of shape coefficient at each layer. Envelope values are taken in the ranges of 0°-180° and 180°-360°. It can be seen that (1) in the range of $\theta \leq 60°$ along the circumferential direction, different four-tower arrangements have little impact on the average wind pressures; (2) in the range of $60° \leq \theta \leq 100°$, the site of maximum negative pressure in the single-row arrangement and oblique L-shaped arrangement occurs at a higher circumferential angle as compared with the single tower. The maximum negative pressure occurs at a circumferential angle of 80°, and its value is higher by 42% and 11% respectively as compared with the single-tower arrangement. The distribution patterns of wind pressure for the rectangular, rhombic and L-shaped arrangements are similar to that of the single tower. The average wind pressure of the rhombic arrangement is slightly smaller than that of the single tower; the average wind pressure of the L-shaped pattern is slightly higher than that of the single tower; (3) in the region of flow separation and leeward region ($100° \leq \theta \leq 300°$), the average wind pressures vary significantly under different arrangements. As compared with the single tower, the single-row, rectangular, rhombic, L-shaped and oblique L-shaped arrangements show an increase by 93%, 38%, 50%, 19% and 56%, respectively. The point of separation is delayed under the L-shaped arrangement.

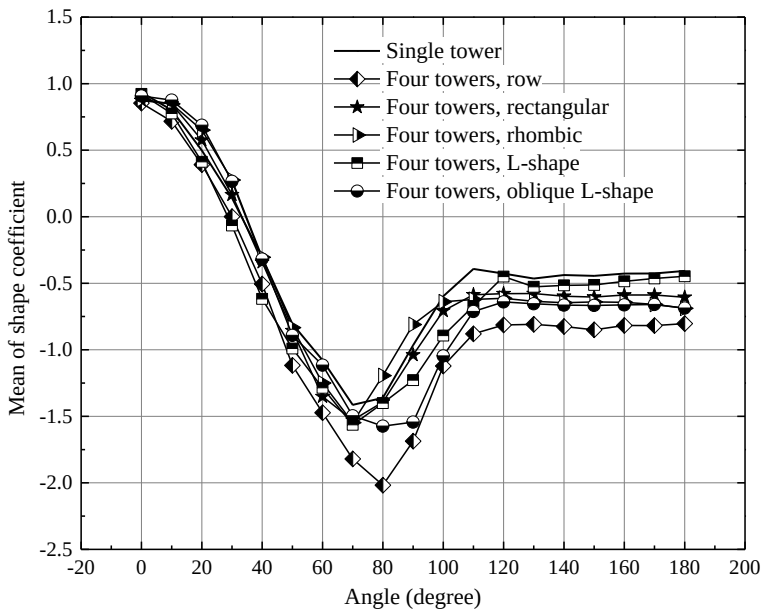

Fig. 10 Distribution curves of 2D shape coefficient of single-tower arrangement and five typical four-tower arrangements under the most unfavorable working conditions

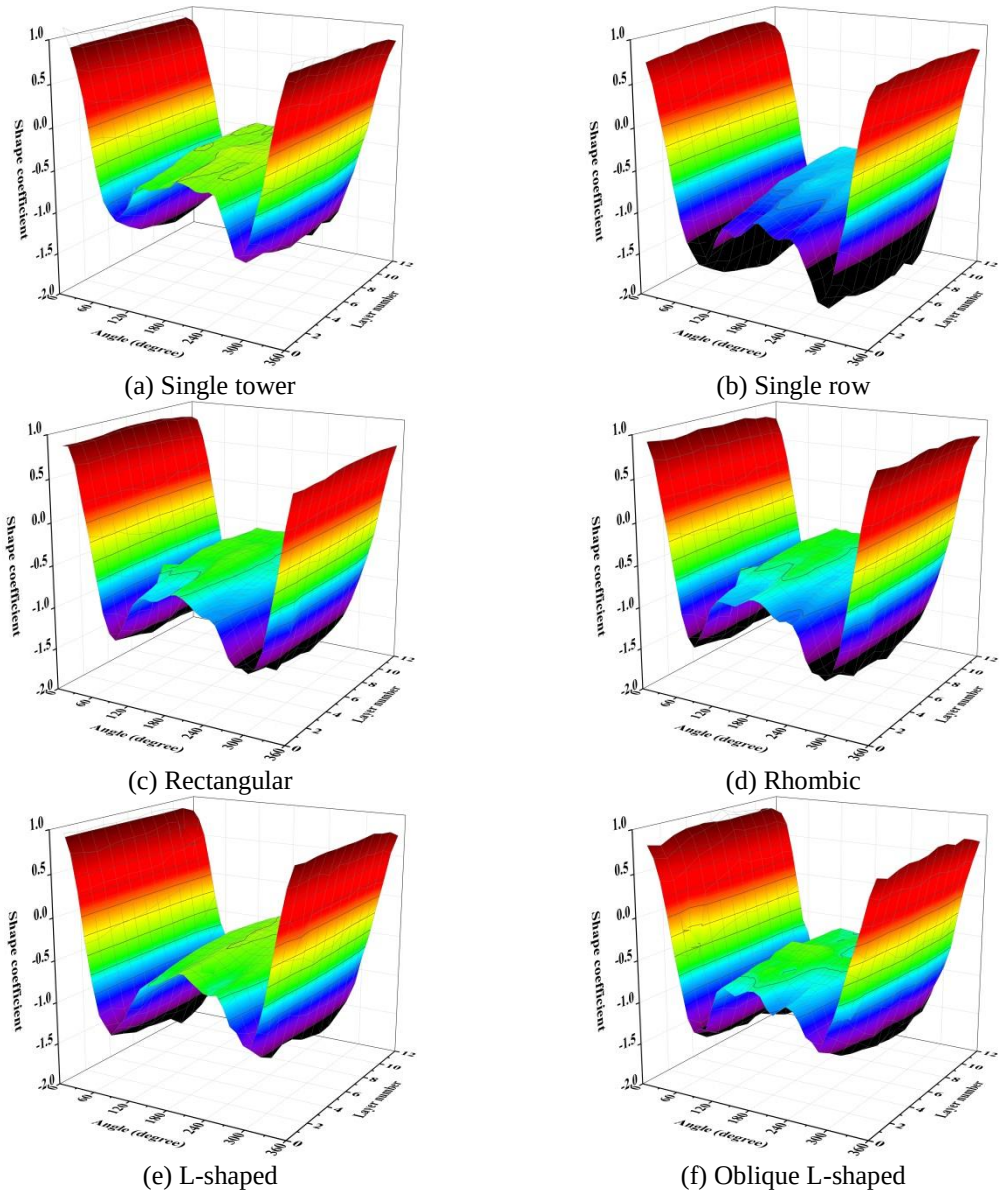

(a) Single tower (b) Single row

(c) Rectangular (d) Rhombic

(e) L-shaped (f) Oblique L-shaped

Fig. 11 3D distribution of shape coefficient of single-tower arrangement and five typical four-tower arrangements under the most unfavorable working conditions

Fig. 11 shows the 3D distributions of shape coefficient of single-tower arrangement and five typical four-tower arrangements under the most unfavorable working conditions. Comparison shows that (1) the distribution of average wind pressure at the bottom of the tower under the five four-tower arrangements is significantly different as compared with the single tower. The bottom effect is conspicuous for the cooling towers due to the group tower-related interference; (2) the

maximum positive pressure on the cooling towers varies little under different four-tower arrangements. Regions of maximum negative pressure and leeward regions are the most affected by the interference effect; (3) the average wind pressure under the single-row arrangement is most affected by the interference effect. The absolute values in the regions of maximum negative pressure and leeward regions increase dramatically. However, the distribution pattern of average wind pressure remains symmetrical; (4) Bulging is observed in the leeward regions under the most unfavorable working conditions for rectangular, rhombic, L-shaped and oblique L-shaped arrangements.

4.2 Pulsating wind loads

Fig. 12 shows curve of pulsating wind pressure of single tower measured by wind tunnel test and the curves obtained by using different techniques of measurement (Ruscheweyh 1975, Sageau 1980, Sun *et al*. 1992, Cheng *et al*. 2015). The distribution curve of pulsating wind pressure along the circumferential direction could be divided into three regions: along-wind region ($0°\leq\theta\leq40°$), cross-wind region ($40°\leq\theta\leq120°$) and leeward region ($120°\leq\theta\leq180°$). For the along-wind region, the pulsating wind pressure is the highest at the direct along-wind point. Cross-wind region has the most violent fluctuation of pulsating wind pressure on the surface of the cooling tower, with the maximum occurring near the circumferential angle of 80°. The region of 100°-120° is the transition between the cross-wind region and wake region, where the pulsating wind pressure drops sharply. The wind pressure in the leeward region fluctuates mildly and its value is low. Comparison shows that the distribution curve of pulsating wind pressure coefficient more coincides with the curve measured by using Ruscheweyh's method and the former is located within the envelope curves of the four measurements. This verifies the reliability of using wind tunnel test to obtain the pulsating wind loads on the surface of the cooling tower.

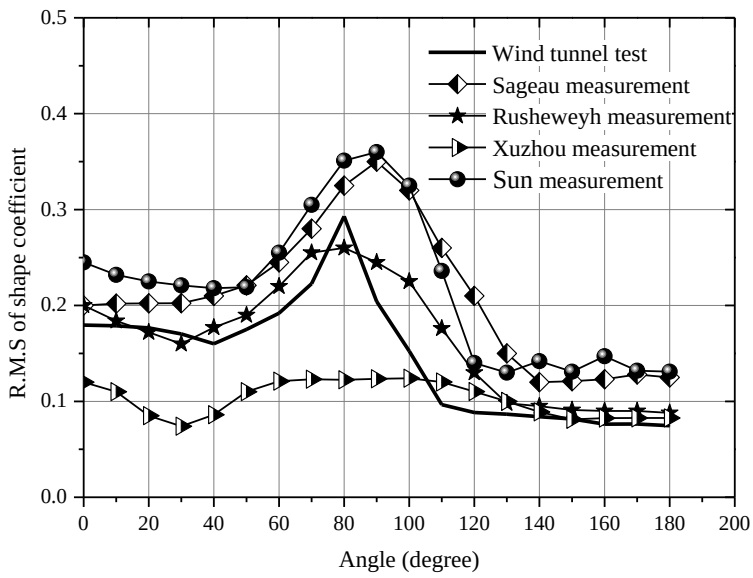

Fig. 12 Comparison of wind tunnel test results and actual measurements of 2D pulsating wind pressure coefficient for the single tower

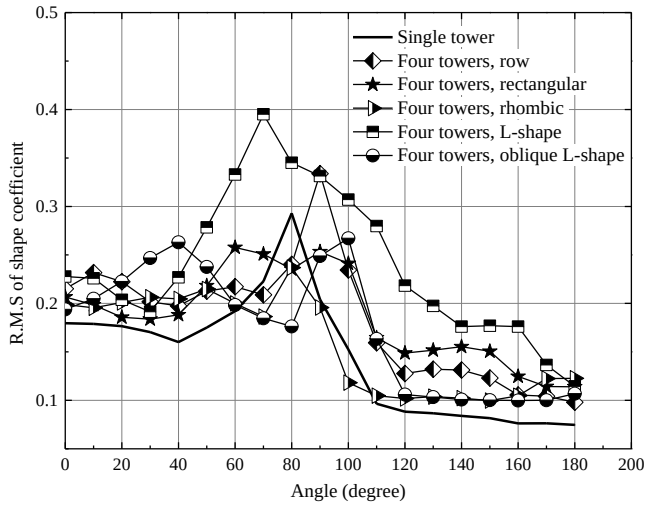

Fig. 13 Distribution curve of 2D pulsating pressure of the cooling tower for different arrangements under the most unfavorable working conditions

Fig. 13 shows the curves of 2D pulsating wind pressure of single-tower arrangement and five four-tower arrangements under the most unfavorable working conditions. Pulsating wind pressure, average speed of the incoming flow, turbulence intensity and integral scale of the target tower are greatly affected by the specific layout of the four towers. Comparison shows that (1) the average pulsating wind pressures under different four-tower arrangements increase to varying degree as compared with the single tower. It is higher by 26%, 29%, 9%, 57% and 20% under the single-row, rectangular, rhombic, L-shaped and oblique L-shaped arrangements, respectively; (2) cross-wind regions are the most affected under different four-tower arrangements; large differences are observed in the angle at which the maximum pulsating wind pressure occurs under different four-tower arrangements; (3) in contrast, in the leeward regions under the single-row, rectangular, rhombic and oblique L-shaped arrangements, the pulsating wind pressure is distributed more uniformly, and the highest value occurs under the L-shaped arrangement.

Fig. 14 shows the 3D nephograms of pulsating wind pressure of single tower and five four-four arrangements under the most unfavorable working conditions. Axial symmetry can be observed of pulsating wind pressure distribution for the single tower. The first peak region occurs at the wind angle of 70°-90°. As the circumferential angle increases, the pulsating wind pressure decreases dramatically. There is no apparent peak region of pulsating wind pressure in the lower part of the tower for the single tower; near the point of separation there is a rebound. Comparison between Figs. 14(b)-14(f) and 14(a) indicates that (1) asymmetric distribution of pulsating wind pressure is observed due to the interference imposed by the surrounding towers. The area of the asymmetric distribution region is the smallest under the oblique L-shaped arrangement; (2) the distribution patterns of pulsating wind pressure are similar under the rectangular, rhombic and L-shaped arrangements, with the smallest peak region observed under the L-shaped arrangement; (3) the distribution of pulsating wind pressure in the lower part of the tower is considerably affected by the interference imposed by the surrounding towers. This is the region where the peak pulsating wind pressure of the entire tower is likely to occur.

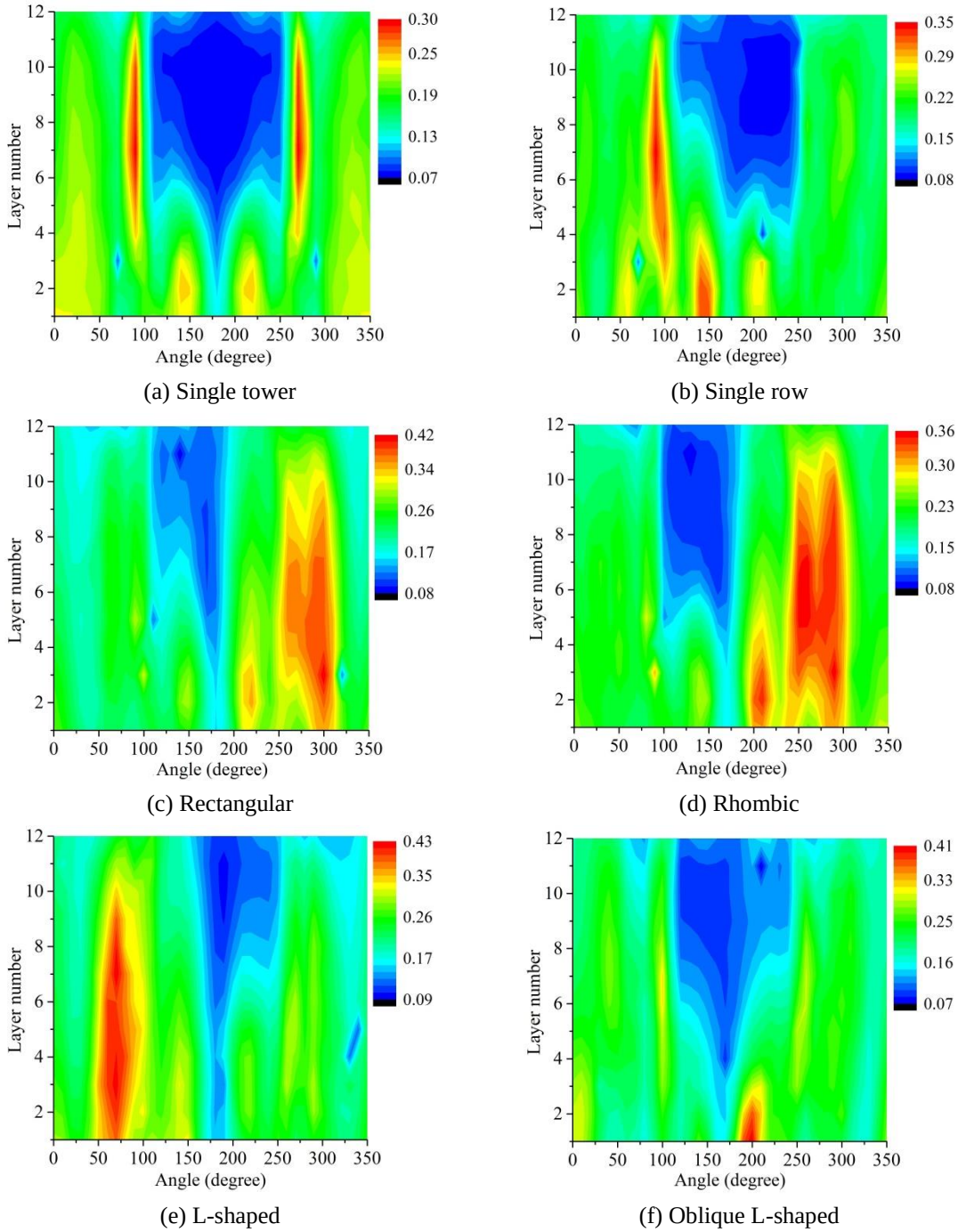

(a) Single tower (b) Single row

(c) Rectangular (d) Rhombic

(e) L-shaped (f) Oblique L-shaped

Fig. 14 3D nephograms of pulsating wind pressure for different arrangements under the most unfavorable working conditions

5. Estimation of multi-dimensional extreme aerodynamic loads

5.1 Non-Gaussian distribution features of wind pressure signals

Fig. 12 shows the probability density curves of wind pressure signals at the point of separation at the throat for the single tower and five typical four-tower arrangements under the most unfavorable working conditions. It can be seen that the wind pressure signals deviate from the standard Gaussian distribution. Further analysis of the probability densities curves indicated a large proportion of wind pressure signals with large skewness and large peak due to the interference effect under the four-tower arrangements.

According to some researches (Zareifard and Khaledi 2013, Ke and Ge 2015), wind pressure signals with $-0.5 \leq \mu_{ssk} \leq 0.5$ and $2 \leq \mu_{sku} \leq 4$ are considered Gaussian (where μ_{ssk} and μ_{sku} are the skewness and kurtosis of wind pressure signals, respectively). Fig. 16 is the relationship between skewness vs. kurtosis of all measuring points for single tower and different four-tower arrangements under the most unfavorable working conditions, respectively. The distributions of skewness and kurtosis are more concentrated in the single-tower arrangement, single-row arrangement and oblique L-shaped arrangement. Under the five typical four-tower arrangements, 30%, 44%, 42%, 51% and 35% of all wind pressure signals are non-Gaussian, whereas in the single-tower arrangement, only 20% of the wind pressure signals are non-Gaussian.

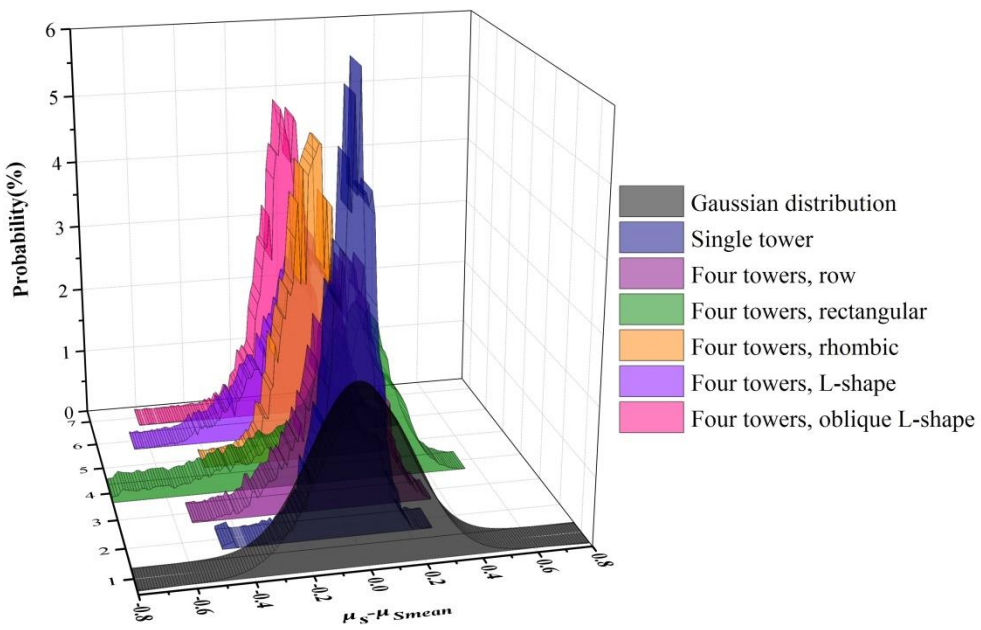

Fig. 15 Probability density curves of wind pressure signals at the point of separation at the throat for the single tower and five typical four-tower arrangements under the most unfavorable working conditions

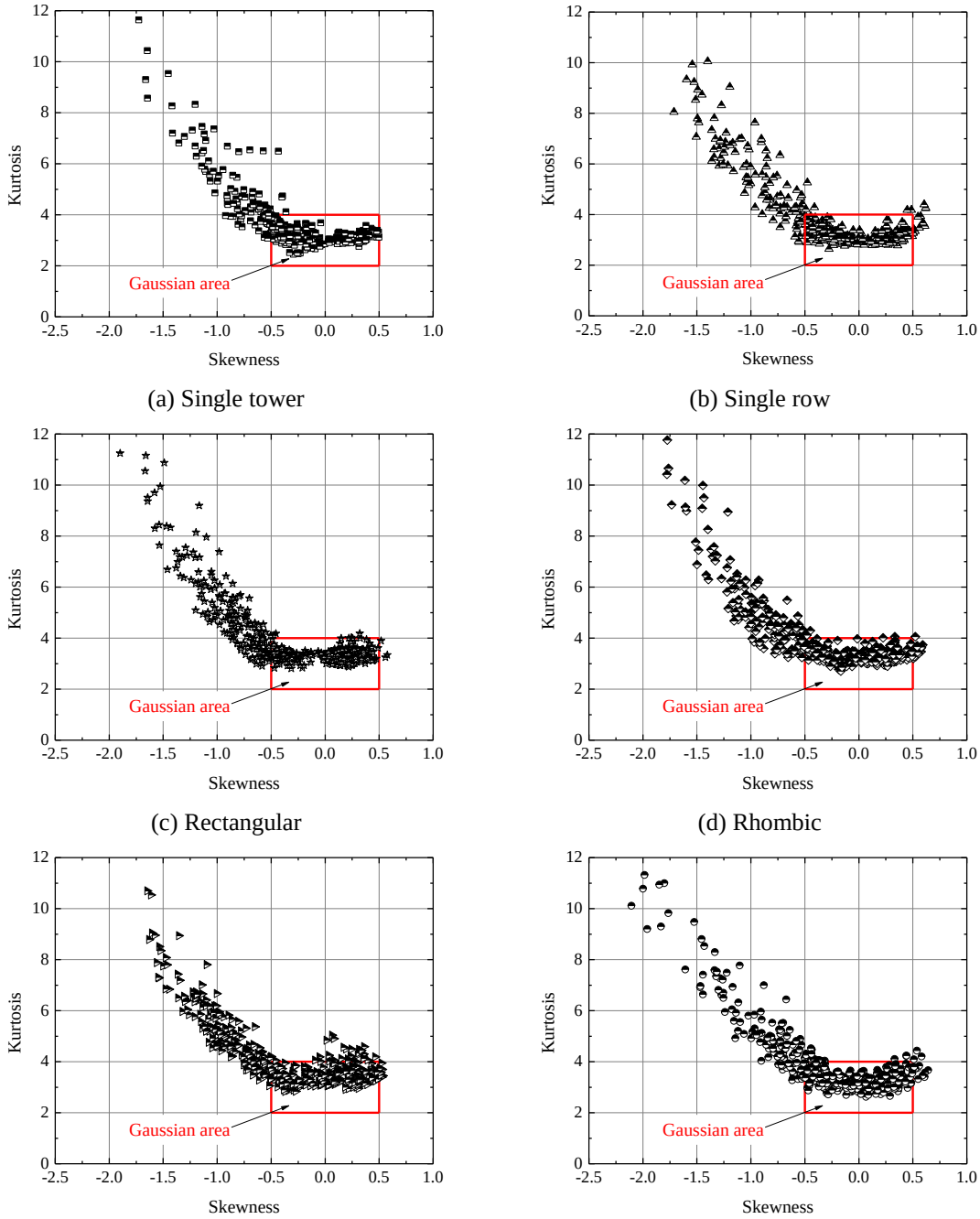

(a) Single tower (b) Single row

(c) Rectangular (d) Rhombic

(e) L-shaped (f) Oblique L-shaped

Fig. 16 Relationship between skewness and kurtosis of wind pressure signals in the single-tower arrangement and different four-tower arrangements under the most unfavorable working conditions

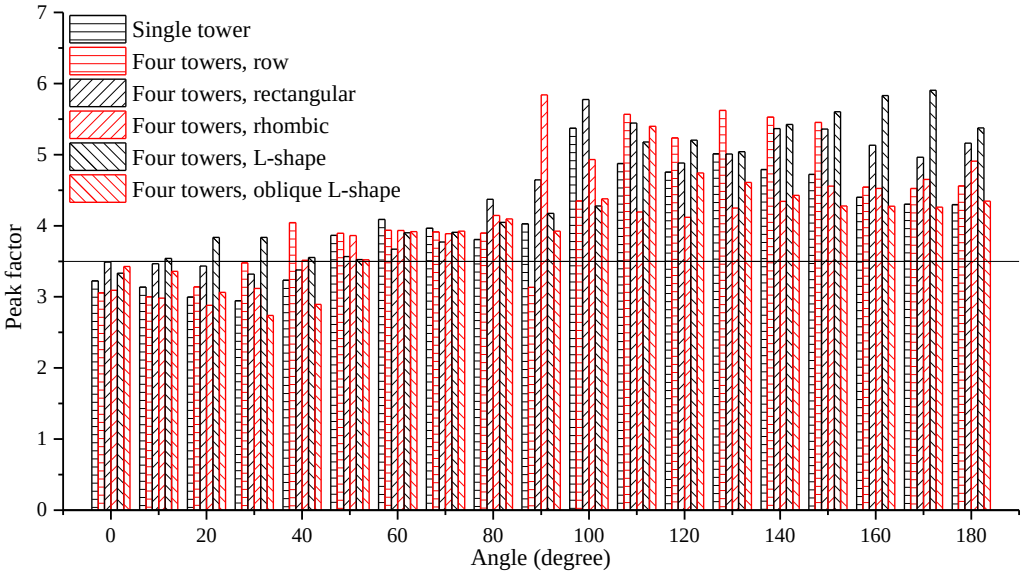

Fig. 17 2D distribution of peak factor in single tower and different four-tower arrangements under the most unfavorable working conditions

Fig. 17 shows the 2D distributions of peak factors calculated using Sadek-Simiu method (Sadek and Simiu 2002, Ding and Chen 2014). The straight line represents the uniform value of peak factor, which is 3.5 according to the Load Code for the Design of Building Structures (GB50009-2012, 2012). It can be seen from the figure that (1) except for the along-wind region ($0°\leq\theta\leq40°$) where the peak factor is below 3.5, the peak factors in the cross-wind region ($40°\leq\theta\leq120°$) and leeward region ($120°\leq\theta\leq180°$) all deviate considerably from the standard value. In these two regions, pulsating wind pressures account for a large proportion of extreme wind pressures, so the use of a standard peak factor will result in severe underestimation of the extreme wind pressures; (2) Of different four-tower arrangement, peak factor distributions of single-row arrangement and oblique L-shaped arrangement are closer to that of the single tower; in contrast, the peak factors of the other three four-tower arrangements increase about 10% as compared with the single tower.

Fig. 18 shows the equipotential lines of peak factor in single tower and different four-tower arrangements under the most unfavorable working conditions. The peak factor distribution on the surface of the cooling tower is asymmetric, with the maximum value occurring at the bottom of the tower which is because the average mean wind pressure here is small. Except for the single-row arrangement where the maximum peak value is above 6.5, the peak factor distributions in the rectangular, rhombic and L-shaped arrangements display a similar pattern; the peak values occur at the bottom of the tower and near the throat in these arrangements. The peak factor reaches the maximum of 7.6 at the bottom of the tower in the oblique L-shaped arrangement, and it is below 6 at other positions.

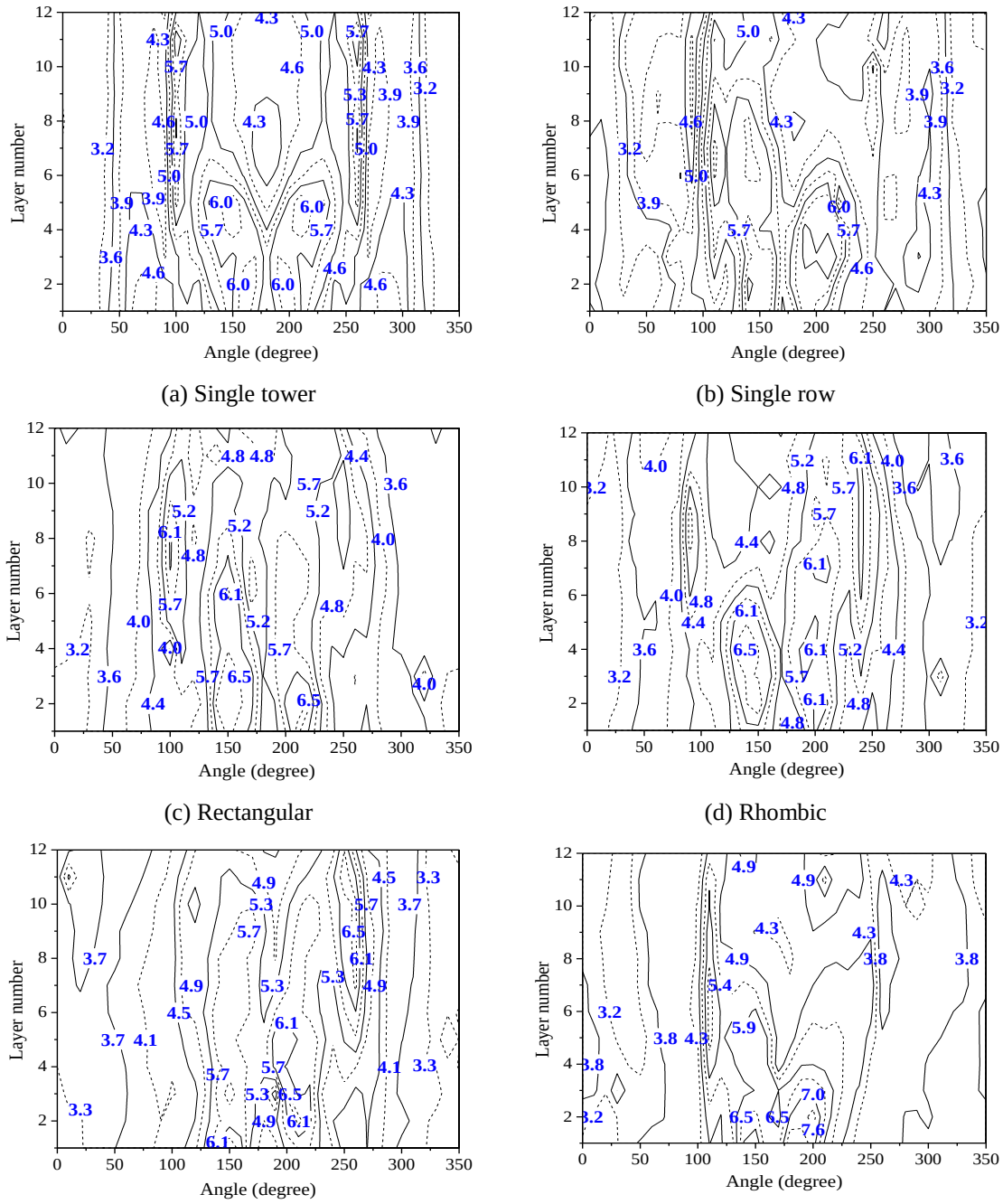

(a) Single tower

(b) Single row

(c) Rectangular

(d) Rhombic

(e) L-shaped

(f) Oblique L-shaped

Fig. 18 Equipotential lines of peak factor under different arrangements

5.2 Extreme wind loads

Distribution curves of 2D extreme shape coefficient of the cooling tower in different arrangements were calculated according to Eq. (1) and Fig. 19. It can be seen that (1) the extreme wind pressures of the along-wind region ($0°\leq\theta\leq40°$) under the four-tower arrangements are similar to those for the single tower; (2) the cross-wind region ($40°\leq\theta\leq120°$) is the region where the points of maximum negative pressure and separation occur in the circumferential direction. The wind angle at which the maximum negative pressure occurs differ across the four-tower arrangements, but it all lies within the range of 70°-90°. The average extreme wind pressures in the cross-wind region under the single-row, rectangular, rhombic, L-shaped and oblique L-shaped arrangements increase by 39%, 19%, 11%, 49% and 22%, as compared with the single tower; (3) extreme wind pressures in the leeward region ($120°\leq\theta\leq180°$) are significantly influenced by the interference effect under the group tower arrangements. As compared with the single tower, the extreme wind pressures in the leeward regions under different four-tower arrangements increase at least by 30%.

Fig. 20 shows the distribution curves of 3D shape coefficient of cooling tower under different arrangements. Comparison will reveal that (1) the distribution pattern of extreme wind pressures in the single-row arrangement is close to that of the single-tower arrangement. Since the number of interference towers on the left and right sides of the target tower is different, the degree of influence related to canyon effect on the extreme wind pressures on the two sides also varies. The distribution pattern of extreme wind pressures is asymmetric; (2) the distribution patterns of extreme wind pressures on the cooling tower are similar under the rectangular and rhombic arrangements. The degree of asymmetry increases regarding the distribution of extreme wind pressures as compared with the single-row arrangement; (3) L-shaped arrangement leads to the largest extreme negative pressure on the surface of the cooling tower among five four-tower arrangements (-3.46). The largest extreme negative pressure occurs near the throat, where the wall thickness is the smallest; (4) the extreme wind pressures on the cooling tower are the smallest in the oblique L-shaped arrangement.

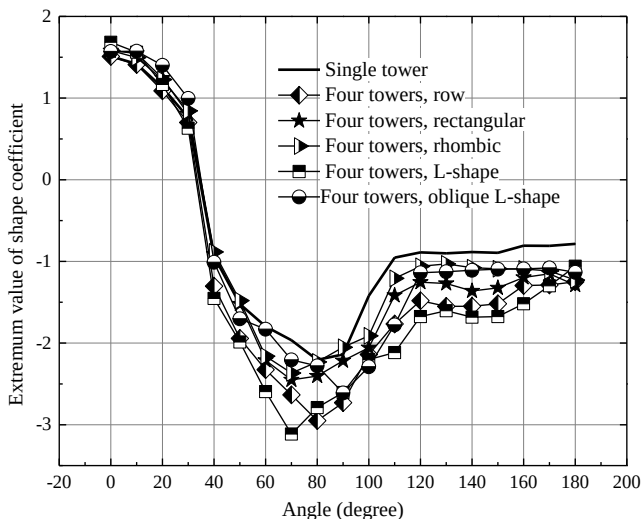

Fig. 19 Distribution curves of 2D extreme shape coefficient of cooling tower under different arrangements

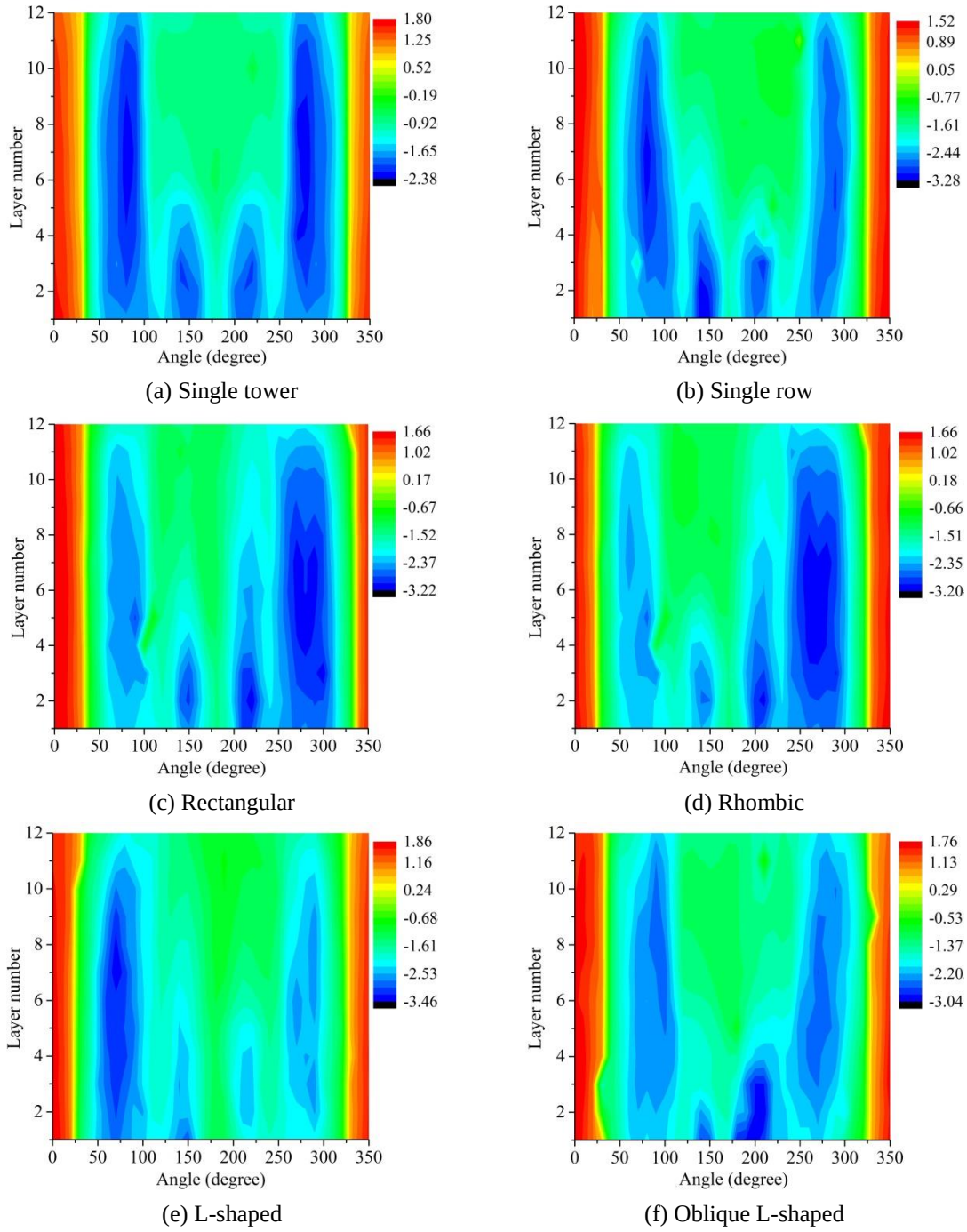

(a) Single tower (b) Single row

(c) Rectangular (d) Rhombic

(e) L-shaped (f) Oblique L-shaped

Fig. 20 Diagrams of extreme 3D shape coefficient under different arrangements

5.3 Evaluation of extreme wind loads

The existing design codes for cooling towers (DL/T 5339-2006 2006, GB/T 50102-2014, 2014, VGB-Guideline 2005) only provide the 2D average wind pressure curve under the single-tower arrangement. However, in engineering design, this average wind pressure curve is usually multiplied by the standard wind-induced vibration factor and interference factor to obtain the extreme wind pressure of the cooling tower under the interference from the surrounding towers. This method of calculating extreme wind loads is not reasonable (Ke and Ge 2015). Therefore, we proposed an evaluation method of extreme wind loads based on experimental measurements under the typical four-tower arrangements.

The equations of 2D extreme wind pressure on the cooling tower for the single-tower and four-tower arrangements were fitted by using the circumferential angle ($0 \leq \theta \leq 360$, unit °) as the objective function. Fig. 21 shows the fitted equations of extreme wind pressure under different arrangements and the distributions of the measured values, with the fitting parameters given in Table 2. The goodness-of-fit (i.e., coefficient of determination R^2) lies between 0 and 1. The closer the value to 1, the better the fitting is. Error analysis of the uniform fitted equations is shown in Fig. 22. The experimental values are evenly distributed around the fitted straight line, which indicate the high predictive capacity of the fitted equations.

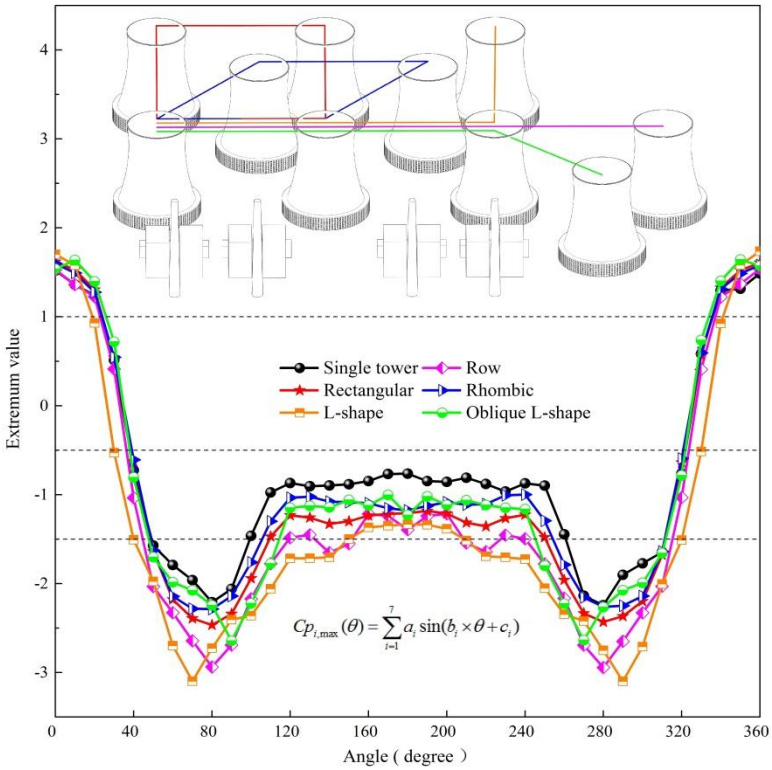

Fig. 21 Uniform fitted equations of 2D extreme wind pressure coefficient and distributions of the measured data under different arrangements

Table 2 Parameters of the uniform fitted equations of 2D extreme wind load on the surface of the cooling tower under the four-tower arrangements

Fitting parameter	Single tower	Single row	Rectangular	Rhombic	L-shaped	Oblique L-shaped
a_1	1.154	2.084	1.776	6.306E-1	2.202	1.984
b_1	6.297E-3	9.427E-3	9.322E-3	1.096E-2	8.889E-3	1.152E-2
c_1	-2.704	-3.268	-3.249	-4.993	3.113	-3.641
a_2	1.212	1.240	1.125	1.069	1.290	1.330
b_2	4.016E-2	3.276E-2	3.484E-2	3.003E-2	3.792E-2	2.989E-2
c_2	6.234E-1	1.957	1.584	2.451	1.019	2.477
a_3	1.187	5.829E-1	6.957E-1	5.966E-1	1.013	4.583E-1
b_3	5.267E-2	5.275E-2	5.197E-2	0.568E-1	4.767E-2	5.643E-2
c_3	1.517	1.503	1.640	7.728E-1	2.409	8.481E-1
a_4	2.054	1.984E-1	1.638E-1	1.731E-1	1.744E-1	4.341
b_4	1.527E-1	8.463E-2	8.384E-2	7.765E-2	7.435E-2	1.307E-1
c_4	-3.925	-1.102	-1.001	1.728E-1	7.716E-1	-3.100
a_5	0.286	1.245	5.277E-1	4.722	4.476E-1	4.324
b_5	0.676E-1	1.315E-1	1.311E-1	1.337E-1	2.709E-2	1.314E-1
c_5	1.984	-0.115	-3.172	-3.654	-3.287	-8.598E-2
a_6	2.031	1.183	5.486E-1	4.745	2.506	4.424E-2
b_6	1.538E-1	1.299E-1	1.339E-1	0.134	1.826E-1	0.156E-1
c_6	5.320	-2.966	-5.119E-1	-0.563	-3.013	1.780
a_7	1.022E-1	1.044E-1	-04.723E-3	1.836	2.476	9.134E-2
b_7	1.004 E-1	0.187	1.016E-2	1.093E-2	1.833E-1	2.747E-1
c_7	2.368	2.482	-2.756E-1	3.096	-4.678E-4	-0.830
Goodness-of-fit	9.944 E-1	9.933 E-1	9.930 E-1	9.915E-1	9.905 E-1	9.944 E-1

Extreme wind loads vary significantly at different heights of the super-large cooling towers, especially at the throat and top. However, the effect of height on the design wind loads tends to be neglected, and this does not conform to the actual distribution of extreme wind loads. In order to determine the range of extreme wind pressures on the surface of cooling tower under single-tower arrangement and four-tower arrangements, we fitted the distribution of 3D extreme wind pressure using non-linear least-squares method. Taking the height ratio *n* along the meridional direction and

circumferential angle θ as objective function, the equations for estimating extreme wind pressures under different arrangements are provided below

$$\begin{aligned} Cp_{i,\max}(n,\theta) = {} & a_{00} + a_{01}n + a_{02}n^2 + a_{03}n^3 + a_{04}n^4 + a_{05}n^5 + a_{10}\theta + a_{11}\theta n + a_{12}\theta n^2 + a_{13}\theta^1 n^3 + a_{14}\theta n^4 + a_{20}\theta^2 \\ & + a_{21}\theta^2 n + a_{22}\theta^2 n^2 + a_{23}\theta^2 n^3 + a_{30}\theta^3 + a_{31}\theta^3 n + a_{32}\theta^2 n^2 + a_{40}\theta^4 + a_{41}\theta^4 n + a_{50}\theta^5 \end{aligned} \tag{9}$$

where n=z/H; z is the height of the measuring point; H is the total tower height; a_{ij} is the fitting coefficient; the fitting parameters are given in Table 3.

Table 3 Fitting parameters of uniform equations of 3D extreme wind load under different arrangements

Fitting parameter	Single tower	Single row	Rectangular	Rhombic	L-shaped	Oblique L-shaped
a_{00}	2.343	0.4292	2.311	5.609	1.047	4.03
a_{01}	9.11	18.41	15.65	-12.9	13.86	-10.52
a_{02}	-45.9	-66.38	-78.87	18.01	-49.16	31.41
a_{03}	94.95	121.8	166.4	-3.56	99.46	-30.78
a_{04}	-93.8	-110.7	-160.6	-17.83	-106.1	-5.185
a_{05}	37.41	40.29	58.29	14.63	46.02	16.69
a_{10}	-0.1331	-8.322E-2	-0.1665	-0.2457	-0.1547	-0.1402
a_{11}	-0.1117	-0.338	-0.04481	0.1256	-0.1409	-0.119
a_{12}	0.2855	0.5862	0.1723	0.03339	0.2025	0.1668
a_{13}	-0.2094	-0.4619	-0.1293	-0.09307	-9.501E-3	-0.01736
a_{14}	5.413E-4	0.1234	0.01045	-0.032	-0.1032	-0.1157
a_{20}	1.424E-3	9.162E-4	1.819E-3	3.109E-3	1.904E-3	1.613E-3
a_{21}	5.097E-4	1.857E-3	7.779E-7	-1.227E-3	4.95E-4	9.317E-4
a_{22}	-7.868E-4	-1.499E-3	-4.671E-4	4.371E-4	-8.85E-4	-9.177E-4
a_{23}	5.777E-4	5.107E-4	3.895E-4	4.897E-4	6.264E-4	7.995E-4
a_{30}	-5.855E-6	-3.603E-6	-7.872E-6	-1.67E-5	-8.645E-6	-7.982E-6
a_{31}	-1.121E-6	-4.73E-6	5.541E-7	3.052E-6	-1.055E-8	-2.617E-6
a_{32}	-8.218E-9	1.428E-6	-3.056E-7	-2.234E-6	-3.398E-7	-4.312E-7
a_{40}	8.139E-9	3.723E-9	1.223E-8	3.961E-8	1.424E-8	1.647E-8
a_{41}	1.568E-9	4.183E-9	-9.003E-11	-4.91E-10	1.707E-10	4.029E-9
a_{50}	-1.779E-14	3.55E-12	-2.635E-12	-3.386E-11	-4.569E-12	-1.073E-11

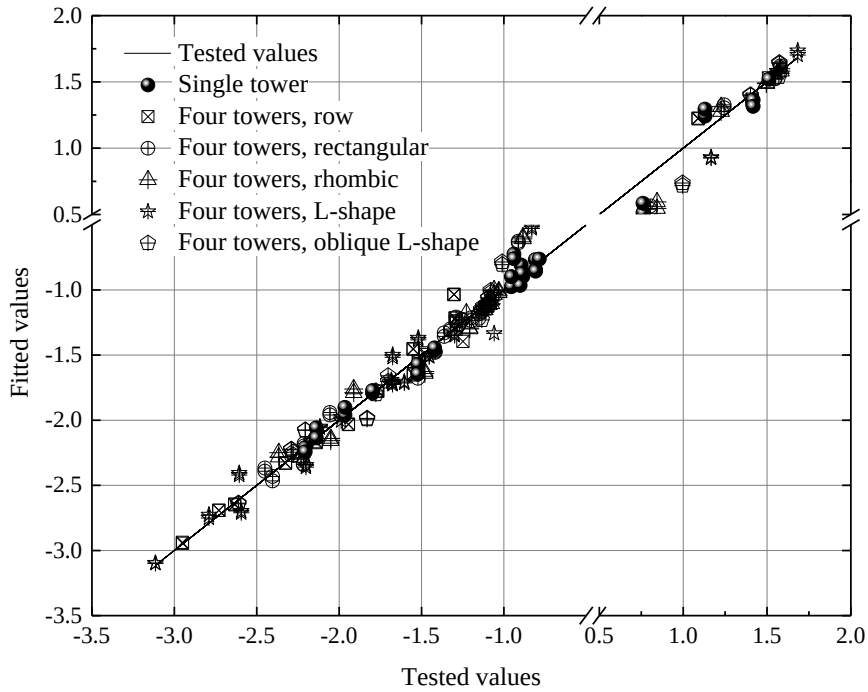

Fig. 22 Schematic of error analysis on the uniform fitted equations of 2D extreme wind pressure coefficient under the four-tower arrangements

Fig. 23 is the schematic of error analysis of the fitted equations of 3D extreme wind pressure. R^2 and Adjusted R^2 are variables that characterize the goodness-of-fit. The closer the value to 1, the better the fitting is. RMSE is root mean square error; the close the value to 0, the better the fitting is. The fitted equations display high predictive power, thus confirming the reasonability of the evaluation method of extreme wind pressures.

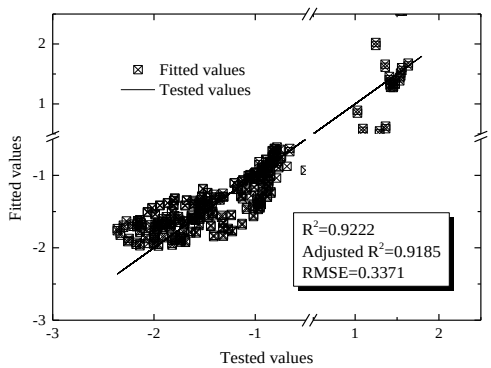

(a) Single tower

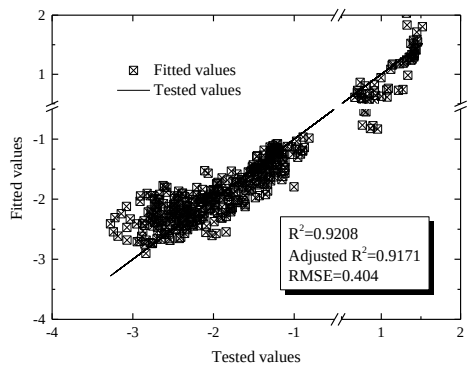

(b) Single row

Continnued-

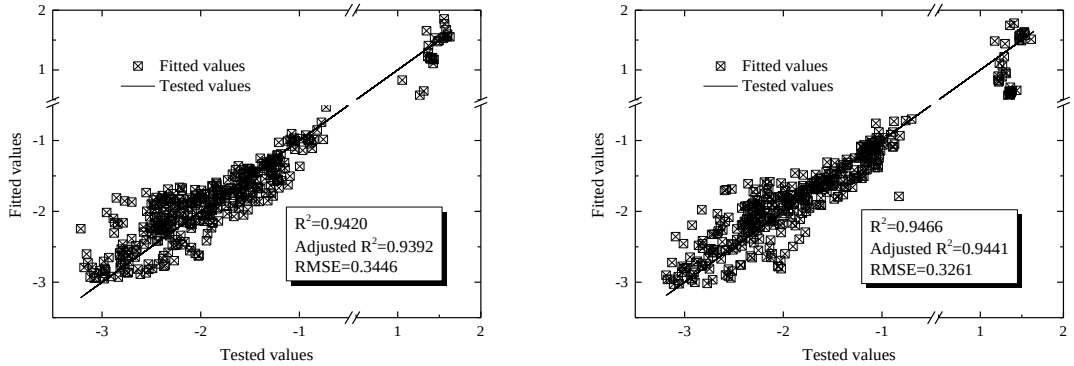

(c) Rectangular (d) Rhombic

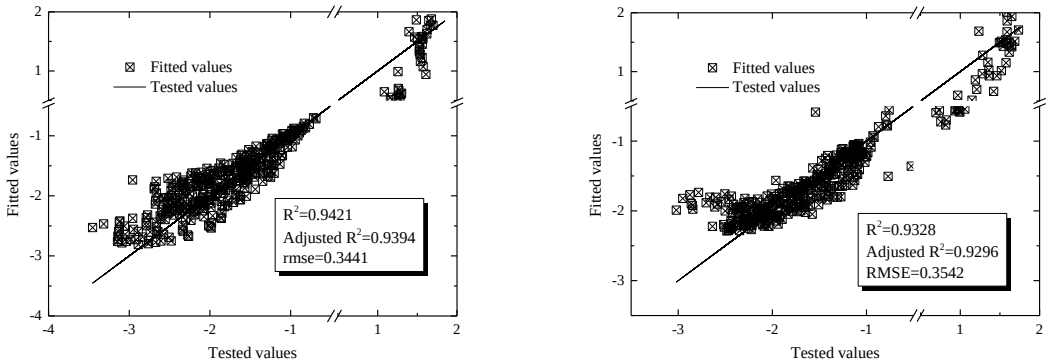

(e) L-shaped (f) Oblique L-shaped

Fig. 23 Schematic of error analysis of the fitted equations of 3D extreme wind pressure coefficient under different arrangements

6. Conclusions

This paper analyzed the effect of different four-tower arrangements on extreme wind loads of the cooling tower and proposed the evaluation method of extreme wind loads. The main contents of the research included wind tunnel test, analysis of interference effect, wind pressure distribution pattern, non-Gaussian distribution feature and extreme wind pressure calculation. We established the uniform fitted equations of multi-dimensional extreme wind pressures (i.e., 2D and 3D wind pressure distributions) on the cooling tower under the interference effect imposed by the surrounding towers using Sadek-Simiu method and non-linear least-squares method. The following conclusions are reached:

- The most unfavorable working conditions were determined based on resultant force coefficient for the five four-tower arrangements. Regression analysis indicated a good linear correlation between the maximum *EIF* and characteristic angle α. The value of maximum *EIF* ranges from 1.278 to about 1.476 for the various four-tower arrangements investigated.
- The interference effect associated with the four-tower arrangements considerably amplified the average wind pressures on the cooling tower. Cross-wind and leeward regions are most affected. As compared with the single tower, the average shape coefficients in the negative

pressure regions under the single-row, rectangular, rhombic, L-shaped and oblique L-shaped arrangements increase by 64%, 20%, 18%, 21% and 34%, respectively. The interference effect greatly influences the distribution pattern of pulsating wind pressures on the cooling tower. This is mainly manifested as local increase of pulsating wind pressure and asymmetry of distribution along the circumferential direction. As compared with the single tower, the average pulsating wind pressures along the circumferential direction under the five four-tower arrangements increase by 26%, 29%, 9%, 57% and 20%, respectively.

- Due to the interference effect, the amount of non-Gaussian wind pressure signals under the single-row, rectangular, rhombic, L-shaped and oblique L-shape arrangements increases by 11%, 63%, 56%, 89% and 30%, as compared with the single tower. The peak factors of the single-row and oblique L-shaped arrangements are less affected by the interference effect, while the peak factors of rectangular, rhombic and L-shaped arrangements increase dramatically; peak factors in some positions of the cooling tower are above 6.5 for the rectangular, rhombic and L-shaped arrangements.
- Negative wind pressures vary significantly due to interference effect. All four-tower arrangements have an increase in negative wind pressure as compared with the single tower. The maximum negative wind pressure in the L-shaped arrangement reaches up to -3.45; the average wind pressures in the leeward regions of single-row, rectangular, rhombic, L-shaped and oblique L-shaped arrangements increase by 66%, 49%, 31%, 74% and 31%, respectively, as compared with the single tower. Amplification of local extreme wind pressures caused by interference effect will exert an adverse impact on the anti-wind safety of the structure.
- The uniform fitted equations of extreme wind pressures under the four-tower arrangements prove to be reliable and effective for predicting the 2D and 3D extreme wind loads for single tower and typical four-tower arrangements. The research findings provide reference for the determination of extreme wind loads of super-large cooling towers in four-tower arrangement.

Acknowledgments

This project is jointly supported by National Natural Science Foundation (51208254 and 51021140005), Jiangsu Province Outstanding Natural Science Foundation (BK20160083), Qing Lan project, and Postdoctoral Science Foundation (2013M530255; 1202006B), which are gratefully acknowledged.

References

ASCE Structural Engineering Institute. (2012), "Wind Tunnel Testing for Buildings and Other Structures", *ASCE 49-12-2012*, The American Society of Civil Engineers.

Bearman, P.W. (1967), "Wind forces and the proximity of cooling towers to each other", *Nature*, **216**(5050), 735.

Brosamler, G.A. (1988), "An almost everywhere central limit theorem", *Mathematical Proceedings of the Cambridge Philosophical Society*, **104**(3), 561-574.

Cheng, X.X., Zhao, L., Ge, Y.J., Ke, S.T. and Liu, X.P. (2015), "Wind pressures on a large cooling tower", *Adv. Struct. Eng.*, **18**(2), 201-220.

Davenport, A.G. (1964), "Note on the distribution of the largest value of a random function with application to gust loading", *Proceedings of the Institute of Civil Engineers*, **28**(2), 187-196.

Ding, J. and Chen, X. (2014), "Assessment of methods for extreme value analysis of non-Gaussian wind effects with short-term time history samples", *Eng. Struct.*, **80**, 75-88.

Ministry of Housing and Urban-Rural Development of People's Republic of China. (2014), "Standard for wind tunnel test of buildings and structures", *JSJ/T 338-2014*, China Building Industry Press. (in Chinese)

Karakas, A.I., Ozgan, K. and Daloglu, A.T. (2016), "A parametric study for free vibration analysis of hyperbolic cooling towers on elastic foundation using consistent FEM-Vlasov model", *Arch. Appl. Mech.*, **86**(5), 869-882.

Ke, S.T., Ge, Y.J., Zhao, L. and Tamura, Y. (2013), "Wind-induced responses characteristics on super-large cooling towers", *J. Central South Univ. Technol.*, **20**(11), 3216-3227.

Ke, S.T., Ge, Y.J., Zhao, L. and Tamura, Y. (2015), "Stability and reinforcement analysis of super-large exhaust cooling towers based on a wind tunnel test", *J. Struct. Eng. - ASCE*, **141**(12), 04015066.

Ke, S.T. and Ge, Y.J. (2015), "Extreme wind pressures and non-Gaussian characteristics for super-large hyperbolic cooling towers considering aero-elastic effect", *J. Eng. Mech. - ASCE*, **141**(7), 04015010.

Li, G., Cao, W.B., Li, G., *et al*. (2013), "Structural analysis and optimization of large cooling tower subjected to wind loads based on the iteration of pressure", *Struct. Eng. Mech.*, **46**(5), 735-753.

Ministry of Housing and Urban-Rural Development of People's Republic of China. (2014), "Code for design of cooling for industrial recirculating water", *GB/T 50102-2014*, China Planning Press. (in Chinese)

Ministry of Housing and Urban-Rural Development of People's Republic of China. (2012), "Lode code for the design of building structures", *GB50009-2012*, China Building Industry Press. (in Chinese)

Moon, S.A., Lee, T.G., Hur, J.H., *et al.* (2008) "Study on the reentering rates of individual cooling towers installed on a building roof", *Heat Mass Transfer*, **44**(11), 1345-1353.

National Development and Reform Commission. (2006), "Code for hydraulic design of fossil fuel power plants", *DL/T 5339-2006*, China Electric Power Press. (in Chinese)

Niemann, H.J. and Kopper, H.D. (1998) "Influence of adjacent buildings on wind effects on cooling towers", *Eng. Struct.*, **20**(10), 874-880.

Orlando, M. (2001), "Wind-induced interference effects on two adjacent cooling towers", *Eng. Struct.*, **23**(8), 979-992.

Pope, R.A. (1994), "Structural deficiencies of natural draught cooling towers at uk power stations. part 1: failures at ferrybridge and fiddlers ferry", *Struct. Build.*, **104**(1), 1-10.

Portela, G. and Godoy, L.A. (2005), "Shielding effects and buckling of steel tanks in tandem arrays under wind pressures", *Wind Struct.*, **8**(5), 325-342.

Rajan, S.S., Babu, G.R., Arunachalam, S., *et al.* (2013), "Interference factors for natural draught cooling towers based on wind tunnel experiments", *Proceedings of the 8th Asia-Pacific Conference on Wind Engineering*.

Ruscheweyh, H. (1975), "Wind loadings on hyperbolic natural draught cooling towers", *J. Wind Eng. Ind. Aerod.*, **1**(5), 335-340.

Sadek, F. and Simiu, E. (2002), "Peak Non-Gaussian wind effects for database-assisted low-rise building design", *J. Eng. Mech. - ASCE*, **128**(5), 530-539.

Sageau, J.F. (1980), "Caractérisation des champs de pression moyens et fluctuants à la surface des grands aéroréfrigérants", *La Houille Blanche*, **20**(1-2), 61-67.

Sun, T.F. and Gu, Z.F. (1995), "Interference between wind loading on group of structures", *J. Wind Eng. Ind. Aerod.*, **54**(55), 213-225.

Swartz, S.E., Chien, C.C., Hu, K.K., *et al*. (1985), "Tests on microconcrete model of hyperbolic cooling tower", *Exp. Mech.*, **25**(1), 12-23.

VGB-Guideline. (2005), "Structural design of cooling tower- technical guideline for the structural design, computation and execution of cooling towers", *VGB-R 610Ue*, BTR Bautechnik bei Kühltürmen, Standard Essen.

Viladkar, M.N., Bhargava, P. and Godbole, P.N. (2006), "Static soil–structure interaction response of hyperbolic cooling towers to symmetrical wind loads", *Eng. Struct.*, **28**(9), 1236-1251.

Wittek, U. and Grote, K. (2015), "Substitute wind concept for elastic stability of cooling tower shells", *Mater. Member Behavior*, 500-513.

Zareifard, H. and Khaledi, M.J. (2013), "Non-Gaussian modeling of spatial data using scale mixing of a unified skew Gaussian process", *J. Multivariate Anal.*, **114**(114), 16-28.

Zhao, L. and Ge, Y.J. (2010), "Wind Loading Characteristics of super-large cooling towers", *Wind Struct.*, **13**(4), 257-274.

CC